Chapter 16

Heat and Fluid Flow in Porous Media for Polymer-Electrolyte Fuel Cells

Prodip K. Das* and Deepashree Thumbarathy

School of Engineering, Newcastle University

Newcastle, NE1 7RU, United Kingdom

Abstract

Polymer-electrolyte fuel cells (PEFCs) have attracted much interest recently as promising green energy sources for portable equipment and automotive applications due to their high efficiency, power density and lack of pollutants. However, the key barrier to their commercial success is due to their high cost, which stems from the need to balance durability, performance, and materials. Thus, there is a pressing need to further understand the complex interactions between the materials and its performance, which can be addressed with better knowledge of heat and fluid flow in the porous layers of PEFCs. This chapter covers, in brief, an overview of PEFCs and their operating principles along with associated transport processes. The chapter subsequently highlights mass and thermal transports through the porous gas-diffusion, catalyst, and microporous layers.

* corresponding author: +44 191-208-6170; prodip.das@newcastle.ac.uk

1. Introduction

Global warming and greenhouse gas (GHG) emissions are two critical issues currently addressed by scientists all over the world. Some GHGs (e.g. CO_2) are emitted to the atmosphere through natural processes and human activities. Among the human activities, internal combustion (IC) engine vehicles are significant producers of harmful greenhouse emissions. For instance, a quarter of domestic CO_2 and other greenhouse gas emissions in the UK come from the IC engines vehicles and drones (www.legislation.gov.uk , www.theccc.org.uk). The amount of greenhouse gas emissions come from the combustion of fossil fuels is about 90 %. Recent research also shows that the amount of CO_2 produces from a small car can be reduced by as much as 72 % when powered by a fuel cell running on hydrogen reformed from natural gas instead of a gasoline IC engine. In addition, the world's fossil fuel reserve is limited; hence, alternative and sustainable energy technologies are required for our next generation.

Zero-emission hydrogen fuel-cell vehicles and drones can reduce GHG emissions due to their ability to efficiently converting the chemical energy of hydrogen fuel to generate electricity without a combustion process. Fuel cells also have a broad range of other potential uses, from small-scale battery replacement applications to multi-MW distributed power generation. For vehicles and drones, polymer-electrolyte fuel cells (PEFCs) are considered as a long-term solution for the decarburization of these sectors due to their capabilities of producing high power densities under a rapid load change condition. Many large vehicle manufacturers and the drone industry are dedicated to hydrogen fuel cell technology, such as Toyota and Hyundai Motor.

In a broader sense, PEFCs can be divided into two categories, gas feed (hydrogen) and liquid feed (methanol). Hydrogen fuel cells can be further subdivided into proton-exchange-membrane fuel cells (PEMFCs) and anion-exchange-membrane fuel cells (AEMFCs). In PEMFCs and AEMFCs, hydrogen and oxygen (or air) are combined electrochemically across a polymer membrane generating electricity, water, and heat. Conversely, in methanol fuel cells, methanol and oxygen (or air) are combined electrochemically for generating electricity, water, and heat. The operation of these fuel cells involves a complex overlap of interrelated physicochemical processes, which include electrochemical reactions as well as transport of ions, electrons, energy, and species in gas and liquid phases across several porous layers. Though a significant improvement has been made over the past decades, transports of heat and fluid flow through the porous players of PEFCs still need attention, as the cost and durability of PEFCs

stifle their commercial utilization (Weber et al. 2014). As the interrelated physicochemical processes of these fuel cells are identical, the discussion in this chapter will focus on PEMFCs with some highlights of AEMFCs.

2. Operation Principle of Polymer-Electrolyte Fuel Cells

The images of a polymer-electrolyte fuel cell (PEFC) stack and single-cell and the schematic of various cell components are shown in Figure 16.1. In a PEFC, anode, electrolyte (membrane), and cathode are sandwiched together, known as a membrane electrode assembly (MEA). Both the anode and the cathode include a gas diffusion layer (GDL) and a catalyst layer (CL). Often a microporous layer (MPL) is sandwiched between GDL and CL for better mass transport. To achieve higher output voltages and higher power, cells can be combined with a large fuel cell stack (Figure 16.1).

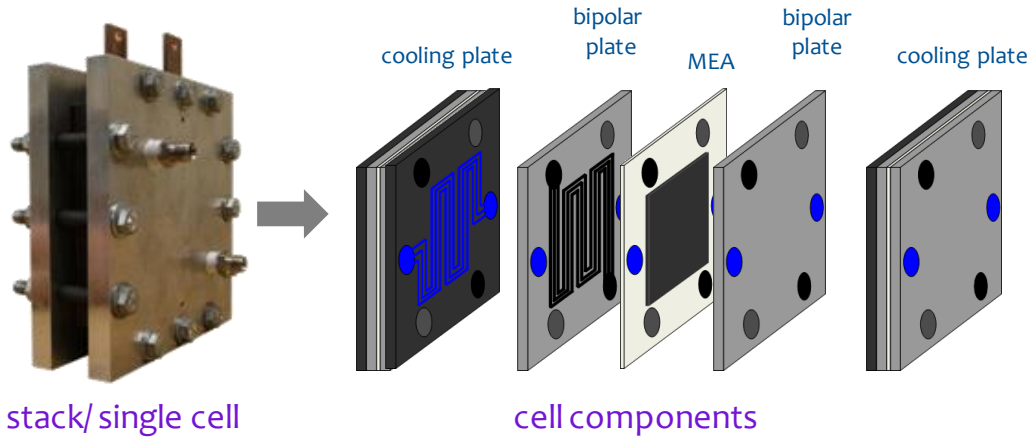

Figure 16.1 – Images of a PEFC stack and single-cell and the schematic of various cell components (image sources: www.fuelcellstore.com and EnSys research group, www.staff.ncl.ac.uk/prodip.das).

Both the PEMFCs and the AEMFCs have identical cell components configuration. The key differences between them are the electrode reactions and the transports of protons and hydroxides ions, as shown in Figure 16.2. In PEMFCs, humidified H_2 gas is supplied into the anode gas flow channel. In the presence of a catalyst, hydrogen molecules are stripped of their electrons to produce protons at the anode catalyst layer (aCL). Then protons transport through a

proton-exchange-membrane (PEM) to the cathode catalyst layer (cCL) and electrons travel through an external circuit to the cathode. At the cCL, protons and electrons recombine with oxygen to generate water. The electrode reactions for PEMFCs are:

$$\text{Anode: } 2H_2 \rightarrow 4H^+ + 4e^- \tag{1}$$

$$\text{Cathode: } 4H^+ + 4e^- + O_2 \rightarrow 2H_2O \tag{2}$$

Conversely, oxygen reduction reaction at the cCL produces hydroxides ions (OH^-) in AEMFCs and then transport through the anion-exchange-membrane (AEM) to the anode. At the aCL, hydroxides ions combine with hydrogen to generate water and electrons. Electrons are then conducted through an external circuit to the cathode to complete the overall cell reaction. The electrode reactions for AEMFCs are:

$$\text{Anode: } 2H_2 + 4OH^- \rightarrow 4H_2O + 4e^- \tag{3}$$

$$\text{Cathode: } O_2 + 2H_2O + 4e^- \rightarrow 4OH^- \tag{4}$$

The aforementioned electrode reactions (Eqs (1)-(4)) are written in a single-step form. However, multiple elementary reaction pathways are possible at each electrode (Li 2006), a discussion of which is beyond the scope of this chapter. For both PEMFCs and AEMFCs, the overall electrochemical reaction can be represented by the following:

$$2H_2 + O_2 \rightarrow 2H_2O + \text{Heat} + \text{Electrical Energy} \tag{5}$$

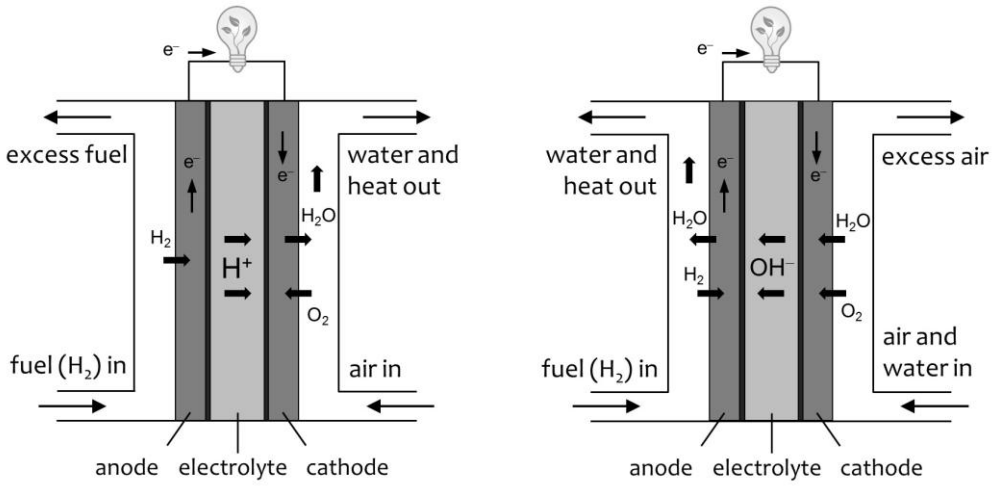

Figure 16.2 – Schematic illustrations of a proton-exchange-membrane fuel cell (left) and an anion-exchange-membrane fuel cell (right).

The electrical energy of a PEFC is estimated from the cell potential and current. While the maximum potential is dictated by the thermodynamics of the reactions, the current is limited by the kinetics and transport limitations within the cell and associated transport losses. Due to the losses (also known as overpotentials), the actual cell voltage is always lower than the equilibrium potential. A typical polarization (potential vs. current density) curve of a PEFC has three distinct regions of losses: activation loss, Ohmic loss, and mass transfer loss. Activation loss is due to the kinetics of charge transfer reactions in aCL and cCL, the Ohmic loss is due to the resistance of cell components, mass transfer loss (concentration overpotential) is due to the limited rate of mass transfer. Figure 16.3 shows a typical performance curve of a PEMFC (also known as polarization curve) and a breakdown of various overpotentials (Das, Li, and Liu 2007, Weber et al. 2014). An AEMFC will exhibit similar curves but the current density values will be lower (Machado, Chakraborty, and Das 2017, Machado et al. 2018).

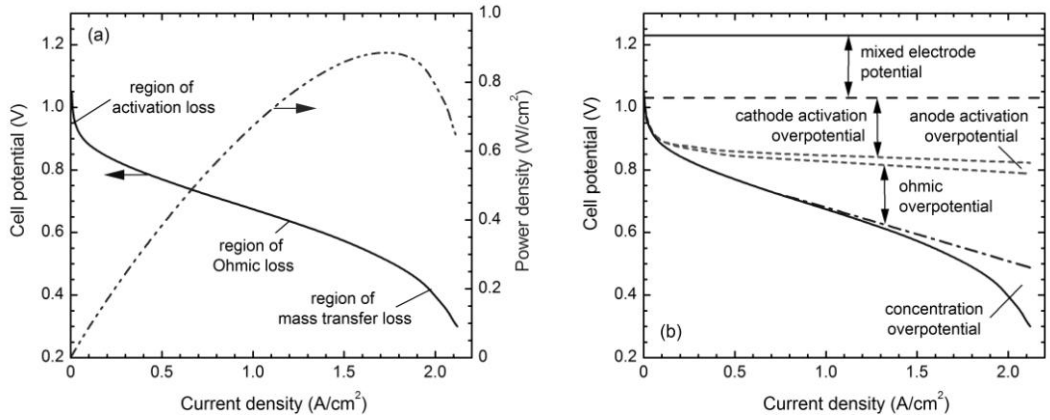

Figure 16.3 – (a) A typical polarization and power density curves for PEMFCs with the region showing three main losses and (b) a breakdown of various overpotentials.

2.1 Operating temperature and pressure

The most important operating parameters for a PEFC operation are temperature and pressure. A PEFC can be operated at room temperature as high as 80 °C, while the operating pressure can be at ambient pressure or at a higher pressure. For the reaction takes place at a

temperature (T) and pressure (p), the maximum potential can be obtained from a PEFC is given by the following expression (Li 2006)

$$E_r^0 = -\frac{\Delta g}{nF} = -\frac{\Delta h - T\Delta s}{nF} \tag{6}$$

where E_r^0 is the standard reversible cell potential, Δg is the change in the Gibbs free energy per mole of H_2, Δh is the enthalpy change per mole of H_2, Δs is the entropy change per mole of H_2, n is the number of electron transfer per mole of H_2, and F is the Faraday's constant. For Eqs. (1) and (3), the value of n is 2. If pure H_2 and O_2 are used as fuel and reactant, the standard reversible cell potential (at 25 °C and 1 atm) will be 1.229 V and 1.185 V for the product water in liquid form and the vapor form, respectively. For higher temperatures, the reversible cell potential will be lower as it decreases with the temperature. On the other hand, the reversible cell potential will be higher at a higher pressure. Although higher operating temperature results in a lower reversible potential, the overall cell performance and the actual cell voltage can be higher at higher temperature due to better reaction kinetics.

2.2 Reactant flow rate and relative humidity

The reactant flow rates and relative humidity also play an important role in the overall performance of a PEFC. Both H_2 and O_2 (or air) are required to be humidified before supplying to the PEFCs for keeping the electrolyte membrane hydrated. Typical relative humidity is about 100% or less. The flow rate of H_2 and O_2 should always be equal or higher than the consumption rates of the fuel and oxidant in a PEFC. The consumption rates ($\dot{N}$) of H_2 and O_2 can be calculated based on the Faraday's law using the following expression:

$$\dot{N}_{\mathrm{H_2,\,consumed}} = \frac{I}{2F} \text{ and } \dot{N}_{\mathrm{O_2,\,consumed}} = \frac{I}{4F} \tag{7}$$

where I is the cell current. Often the actual flow rates are higher than the consumption rates and represented by the parameter called stoichiometry, S_t:

$$S_{t,\mathrm{H_2}} = \frac{\dot{N}_{\mathrm{H_2,\,in}}}{\dot{N}_{\mathrm{H_2,\,consumed}}} \text{ and } S_{t,\mathrm{O_2}} = \frac{\dot{N}_{\mathrm{O_2,\,in}}}{\dot{N}_{\mathrm{O_2,\,consumed}}} \tag{8}$$

For typical PEFC operation, the stoichiometry ratios are about 1.1~1.2 for H_2 and 2 for O_2.

2.3 Thermodynamic efficiency

The theoretical thermodynamic efficiency (also known as reversible efficiency) of a PEFC is defined as the ratio of maximum possible electrical work to the total chemical energy (Li 2006). Thus, we can write

$$\eta_{rev} = \frac{\Delta g}{\Delta h} = 1 - \frac{T\Delta s}{\Delta h} \tag{9}$$

For the standard operating pressure and temperature, the reversible efficiency of a PEFC is about 83%. However, the actual efficiency of a PEFC will be much lower than the reversible efficiency due to the losses illustrated in Figure 16.3.

3. Structures of Porous Media in Polymer Electrolyte Fuel Cells

A rigorous description of PEFC operation requires the coupling of thermodynamics and kinetics of the reactions and conservation of species, energy, and momentum within a representative geometry. A discussion of which is beyond the scope of this chapter and can be found elsewhere (Weber, Balasubramanian, and Das 2012). Thus, the focus is given on the conservation of species, energy, and momentum in this chapter.

To understand the transport of species, energy, and momentum, it is essential to understand the structures of PEFC components and the associated phases. In a PEFC, several phases co-exist together including a liquid phase, a gas phase, and a solid phase. Further, the multi-phase mixture flows through narrow gas channels, porous gas diffusion layers, and porous catalyst layers. Therefore, the governing equations for PEFCs are influenced by the physical structure of the cell and co-existing phases.

The core part of a PEFC has nine layers. Four layers on the anode side and four layers on the cathode side, and a polymer electrolyte layer in the middle. The four layers on each side of the polymer electrolyte layer are a bipolar plate, a GDL, an MPL, and a CL. The flow channels are grooved on the bipolar plate. The average dimensions of the polymer electrolyte layer, CL, MPL, GDL, and flow channel are 50, 10, 40, 200, and 1000 μm, respectively. Each of these layers has several co-existing phases. A schematic illustration of the structures of these layers and various phases is shown in Figure 16.4. The porous media within a PEFC include the CLs

and the diffusion media, which are often composed of multiple layers including GDLs and MPLs. In the following, an overview is given for these porous layers.

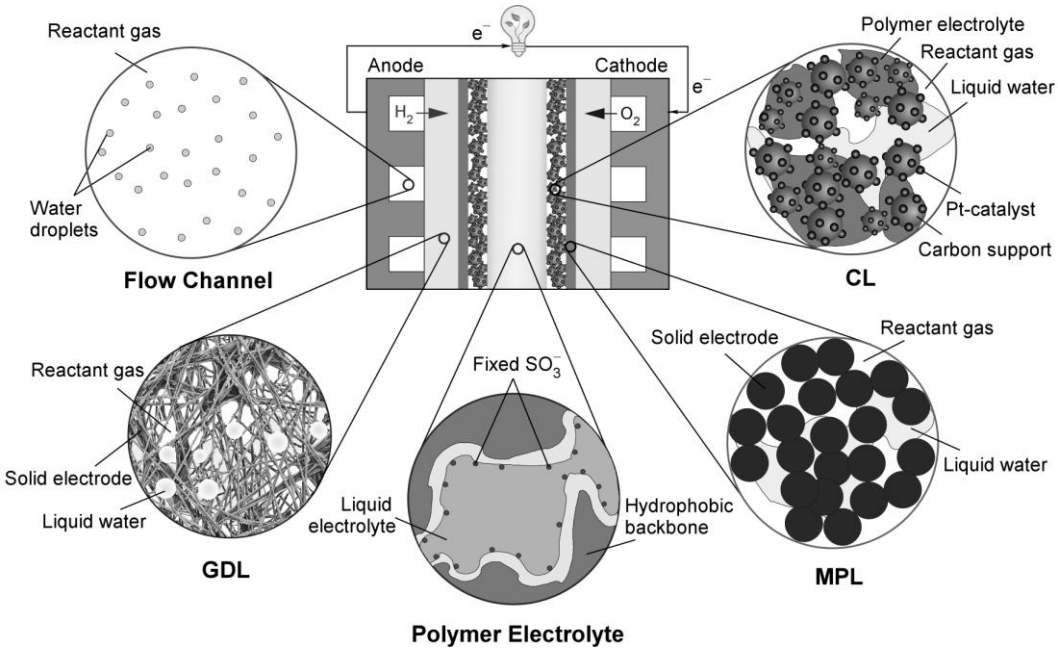

Figure 16.4 – Physical structures of various layers of a PEFC.

3.1 Catalyst layer

PEFCs have two catalyst layers (CLs) where the electrochemical reactions take place. CLs are in direct contact with the polymer electrolyte and MPL, at both anode and cathode sides. These CLs have a complex structure of the membrane, supported carbon particles, catalyst particles, and void space. They must provide void spaces for the reactants to reach the catalyst surface and the products to be escaped. In addition, there should be a pathway for the electrons and protons to reach the reaction sites. The most widely used catalyst layer is the Pt/C CL, where platinum (Pt) nanoparticles dispersed onto the surfaces of larger carbon black particles. The typical pore size in Pt/C CL is about 0.05 μm and the porosity is about 20~30%. The thickness of CLs varies between 10 to 50 μm. The Pt/C CL can have a Pt-loading of several mg per cm^2. Due to the higher cost of Pt catalysts, there is a big push to reduce catalyst loading from the catalyst layers, which leads to the development of the nanostructured thin films (NSTF) catalyst layers.

The key difference of NSTF with conventional Pt/C layers are low Pt-loading, thinner, and no carbon support or ionomer, as the Pt catalyst is directly deposited to form an electronically conductive and electrochemically active layer (Debe 2013, Holdcroft 2014). The NSTF CL is 20 to 30 times (typically 0.5~1 μm) thinner than the conventional Pt/C layer. Thus, it has significantly lower Pt-loading (in the order of 0.05 to 0.15 mg-Pt/cm^2), which would be useful to reduce the cost of a PEFC system. The scanning electron micrographs of conventional Pt/C and NSTF catalyst layers are shown in Figure 16.5.

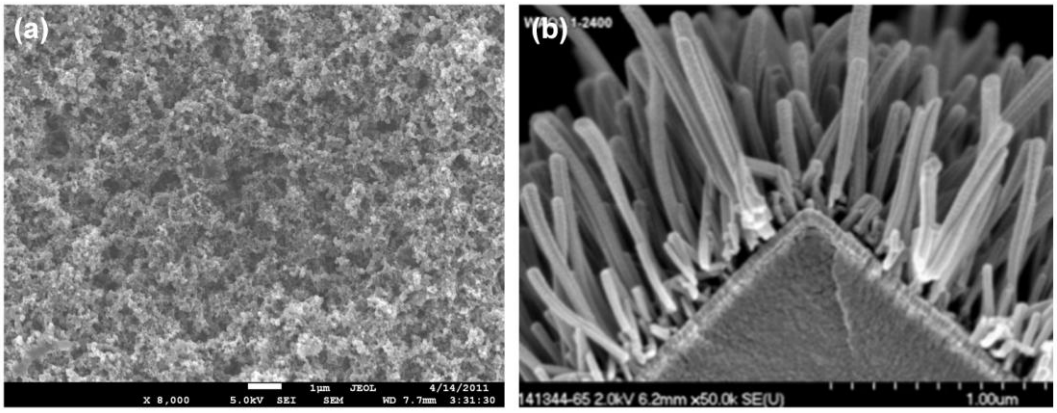

Figure 16.5 – Scanning electron micrographs of (a) conventional Pt/C catalyst layer and (b) NSTF (PtCoMn alloy) catalyst layer (Das and Weber 2013, Debe 2012).

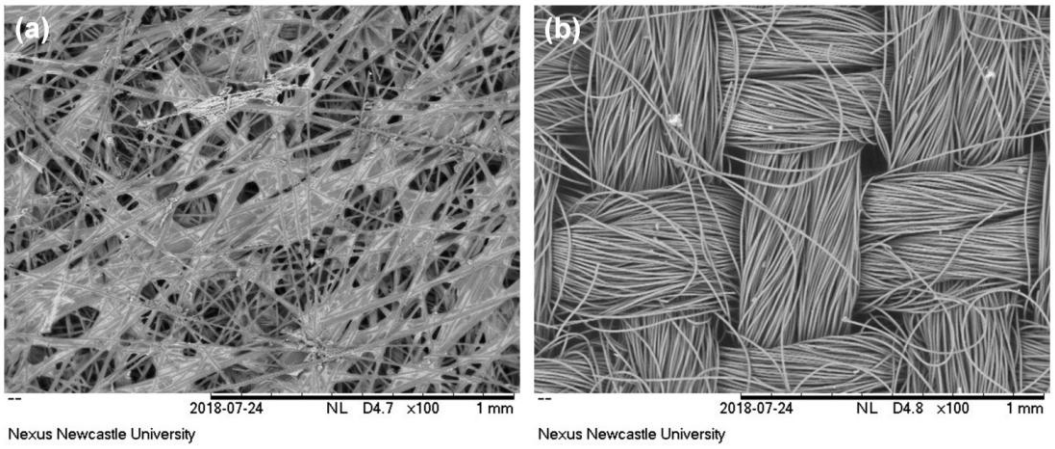

Figure 16.6 – Scanning electron micrographs of typical (a) carbon paper GDL and (b) carbon cloth GDL.

3.2 Gas diffusion and microporous layers

The porous structure of a gas diffusion layer (GDL) is made by weaving carbon fibers into a carbon cloth or by pressing carbon fibers together into a carbon paper. Figure 16.6 shows the scanning electron micrographs of typical carbon paper GDL and carbon cloth GDL. The role of GDLs in PEFCs is to provide mechanical support while spreading the reactant gas and electrons over the electrode as well as allowing the product water to transport from the catalyst layer to the gas flow channel. The GDLs are also rendered wet-proof by saturating the pores with hydrophobic poly-tetra-fluoro-ethylene (PTFE) emulsions, followed by drying and sintering to affix the PTFE particles to the carbon fiber to improve liquid transport, as visible in carbon paper GDL in Figure 16.6a. The typical pore size in GDL is about 10 μm and the uncompressed porosity is about 70~80% (Nam et al. 2009). The thickness of GDLs varies between 100 to 300 μm.

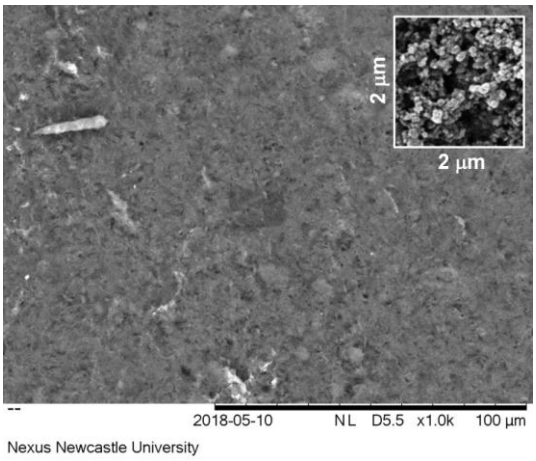

Figure 16.7 – Scanning electron micrograph of a typical microporous layer.

Due to the higher porosity and pore size of GDLs compared with the CLs, most commercial GDLs often come with a microporous layer (MPL), which is a thin layer of carbon nanoparticles mixed with PTFE. For instance, the standard SIGRACET (C-type) MPL is based on 77 wt% carbon black and 23 wt% PTFE. The scanning electron micrograph of a typical microporous layer is shown in Figure 16.7. The MPL acts as a transition layer for the transports of gases and liquid between the macro-pores of GDL and the nano-pores of adjacent CL.

Moreover, MPLs act as a barrier for the liquid water and helps keep the water within the membrane from escaping and prevent drying out the membrane. The typical pore size in MPL varies between 0.1 to 0.3 micron and the porosity is about 50%. The thickness of MPLs varies between 10 to 100 μm. Often the combined layer of the GDL and MPL is referred to as a gas-diffusion electrode (GDE), as the transports through these two layers are fundamentally identical. Thus, the GDL and MPL will be referred to as GDE in the subsequent sections.

4. Transport in Polymer Electrolyte Fuel Cells

The transports of mass, energy, species, electron, and proton in PEFCs involve convection, diffusion, conduction, and migration. In this section, these processes are briefly described for GDE, CL, and membrane, while the transports in the flow channels and solid bipolar plates and the reaction kinetics are available in Ref. (Weber, Balasubramanian, and Das 2012).

4.1 Mass diffusion

The primary mechanism of mass transport inside PEFC porous media is the diffusion. Considering the dilute species transport theory, the flux of species *i* in phase *k* is governed by the Fick's first law

$$\mathbf{N}_{i,k} = -D_i \nabla c_{i,k} \tag{10}$$

where D_i is the diffusion coefficient of species *i* and $c_{i,k}$ is the concentration species *i* in phase *k*. The diffusion coefficient can be predicted from the mean free path and average velocity for molecules in an ideal gas from the Maxwell-Boltzmann distribution and it obeys the following expression

$$D \propto \frac{T^{\frac{3}{2}}}{p} \tag{11}$$

where *T* and *p* are the temperature and pressure, respectively. However, the actual diffusion coefficient in PEFC porous media can be different from the real diffusion coefficient. This is because the available cross-section for diffusion is less than the free fluid, and the distance between one point and another in the porous medium. Thus, the diffusion coefficient should be

corrected using the porosity and tortuosity of PEFC porous media, which is known as the effective diffusion coefficient.

$$D_i^{\text{eff}} = \frac{\varepsilon}{\tau} D_i \tag{12}$$

where D_i^{eff} is the effective diffusion coefficient of species i, ε is the porosity, and τ is the tortuosity. The tortuosity represents the diffusional path that a molecule must travel to cross a region of a certain thickness. The simplest approach to determine the tortuosity is the Bruggeman approximation, which gives

$$\tau = \varepsilon^{-0.5} \tag{13}$$

The Bruggeman approximation has widely been used for estimating the effective transport properties for CLs, GDLs, and MPLs. As the pores of these porous layers can be simultaneously filled with gas and liquid phases, the Bruggeman equation requires to be revised to account for the presence of the liquid phase. Considering the liquid saturation, the Bruggeman equation for two-phase scenarios can be revised as

$$D_i^{\text{eff}} = \varepsilon^m \left(1 - S_l\right)^n D_i \tag{14}$$

where S_l is the liquid saturation, m is the Bruggeman exponent (= 1.5), and n is the saturation exponent. Often the saturation exponent is considered the same as the Bruggeman exponent. However, the value of the saturation exponent is strongly dependent on the amount of liquid saturation (Das, Li, and Liu 2010, Hwang and Weber 2012). At low liquid saturation, the Bruggeman approximation is reasonable but a higher-order correction is needed for the diffusivity at high liquid saturation. It is believed that the Bruggeman approximation underpredicts the diffusion inside the CLs, where the Knudsen diffusion can be significant. Thus, an appropriate measure will be required for the effective diffusion coefficient in CLs to account the Knudsen diffusion as well (Nonoyama et al. 2011).

4.2 Convection

Convection is applicable to both mass and heat transfer. Due to the phase velocities, the fluid (gas or liquid) can be transported through the pores due to the advection. If the phase-velocities are known, one can write the advection transport as

$$\left(\mathbf{N}_{i,k}\right)_{\text{advection}} = c_{i,k}\mathbf{v}_k \tag{15}$$

where $\mathbf{v}_k$ is the mass-averaged velocity of phase *k*. The mass-averaged velocity can be defined using Darcy's law as (Weber et al. 2014)

$$\mathbf{v}_k = -\frac{k_k}{\mu_k}\nabla p_k \tag{16}$$

where k_k is the effective permeability (a product of the absolute permeability and the relative permeability), μ_k is the viscosity, and p_k is the total pressure of phase *k*.

Similarly, the rate of change of thermal energy per unit volume of fluid due to the convection can be written as

$$\dot{\mathbf{q}}'''_{\text{convection}} = \rho_k C_{P_k}\mathbf{v}_k\nabla T_k \tag{17}$$

where ρ_k is the density, C_{P_k} is the heat capacity of phase *k* which is a combination of the various components of that phase, and T_k is the temperature.

4.3 Conduction

Similar to mass diffusion, conduction plays a dominant role in PEFCs. The conduction is involved in the diffusion of thermal energy (as often known as heat conduction), conduction of electron via an external circuit, and conduction of proton via electrolyte membrane. The conduction of proton and electron is discussed later, while the heat conduction is described in this section.

The Fourier's law of thermal conduction governs the heat conduction inside the PEFCs as well as in the solid bipolar plate, which can be written as:

$$\dot{\mathbf{q}}''_{\text{conduction}} = -k^{\text{eff}}_{T,k}\nabla T_k \tag{18}$$

where $\dot{\mathbf{q}}''_{\text{conduction}}$ is the rate of heat transfer by conduction and $k^{\text{eff}}_{T,k}$ is the effective thermal conductivity of phase *k*.

The effective thermal conductivity of PEFC porous media is a function of porosity and thermal conductivity of the solid phase, the gas species, and the liquid water. The simplest approach to estimate the effective thermal conductivity is the Bruggeman approximation, as described earlier. There are many complex and more accurate formulations available in the open literature for effective thermal conductivity (Das, Li, and Liu 2010, Zamel et al. 2010).

Moreover, the thermal conductivity varies significantly within the porous media, which leads to a higher through-plane value than the in-plane value. Thus, careful attention will be required for estimating the effective thermal conductivity and taking care of the anisotropy of the porous media, as the anisotropic effective thermal conductivity can have a strong influence on the temperature profiles inside the GDEs (Pasaogullari et al. 2007).

4.4 Migration and proton transport

Migration takes place in the electrolyte membrane due to the potential difference across the membrane. This is analogous to the diffusion due to the concentration gradient or heat transport due to the temperature gradient. The migration of the charged species in the electrolyte membrane can be written as (Mench 2008)

$$\left(\mathbf{N}_{i,k}\right)_{\text{migration}} = -z_i u_i F c_{i,k} \nabla \Phi \tag{19}$$

where z_i is the charge number for the ionic species, u_i is the mobility of the charged species, F is the Faraday's constant, and $\nabla\Phi$ is the electrical field gradient. The mobility of species i is related to the diffusivity via the Nernst-Einstein relationship as

$$u_i = \frac{D_i}{RT} \tag{20}$$

where D_i is the diffusion coefficient, R is ideal-gas constant (= 8.31 J mole^{-1} K^{-1}), and T is the temperature. Along with the migration, the protons in the membrane can also be transported via diffusion and convection. Combining these three modes of proton transport, we have the Nernst–Planck equation governing the proton transport as (Mench 2008)

$$\mathbf{N}_{i,k} = -D_i \nabla c_{i,k} + c_{i,k}\mathbf{v}_k - z_i u_i F c_{i,k} \nabla \Phi \tag{21}$$

where the first two terms represent the diffusion and convection of protons through the membrane.

4.4 Electron transport

The solid phase of a PEFC consists of a solid electrode and electrolyte membrane phase. The electrons are transported through the solid phase, while the electrolyte membrane acts as an insulator. The transport of electrons is governed by the current balance as

$$\nabla \cdot \left(\sigma_s^{\text{eff}} \nabla \Phi_s \right) = i_h^{rxn} \tag{22}$$

where Φ_s is the electronic potential, σ_s^{eff} is the effective electronic conductivity, and i_h^{rxn} is the overall reaction current density. The effective electronic conductivity takes into account the volume fraction of electronically conductive material in the CLs, GDLs, and MPLs. Similar to other effective properties, the effective electronic conductivity can also be estimated using the Bruggeman correlation as it provides a good approximation of the effective electronic conductivity (Das, Li, and Liu 2010). The overall reaction current density is given by

$$i_h^{rxn} = A_v \left(1 - S_l\right) i_h \tag{23}$$

where i_h is the transfer current density and A_v is the specific interfacial area between the ionically and electronically conductive phases, which can be estimated from (Das, Li, and Liu 2008)

$$A_v = \frac{A_s m_{\text{Pt}}}{\delta_{\text{CL}}} \tag{24}$$

where A_s is the catalyst surface area per unit mass of the catalyst, m_{Pt} is the catalyst mass loading per unit area, and δ_{CL} is the thickness of the catalyst layer. Often the catalyst mass loading is considered uniform throughout the thickness of the CL. However, the distributions of catalyst particles within the CL can be inhomogeneous (Xing et al. 2017, Xing et al. 2018).

For PEFCs, the hydrogen oxidation reaction (HOR) and the oxygen reduction reaction (ORR) occurring at the anode catalyst layer (aCL) and the cathode catalyst layer (cCL), respectively. The transfer current densities (i_h) for these reactions are governed by the Butler-Volmer kinetics, as

$$i_h^{\text{HOR}} = i_0^{\text{HOR}} \left[\frac{p_{\text{H}_2}}{p_{\text{H}_2}^{\text{ref}}} \exp\left(\frac{\alpha_a F \eta_{\text{HOR}}}{RT} \right) - \exp\left(\frac{-\alpha_c F \eta_{\text{HOR}}}{RT} \right) \right] \tag{25}$$

and

$$i_h^{\text{ORR}} = i_0^{\text{ORR}} \left[\exp\left(\frac{\alpha_a F \eta_{\text{ORR}}}{RT} \right) - \frac{p_{\text{O}_2}}{p_{\text{O}_2}^{\text{ref}}} \exp\left(\frac{-\alpha_c F \eta_{\text{ORR}}}{RT} \right) \right] \tag{26}$$

In these equations, i_0 is the exchange current density, α_a and α_c are the anodic and cathodic transfer coefficients, p_{H_2} and $p_{\text{H}_2}^{\text{ref}}$ are the partial pressure and reference partial pressure for H_2, and p_{O_2} and $p_{\text{O}_2}^{\text{ref}}$ are the partial pressure and reference partial pressure for O_2, respectively. The term η represents the overpotential, which can be determined from

$$\eta = \Phi_s - \Phi_m - U_h \tag{27}$$

where Φ_s is the electronic or solid-phase potential and Φ_m is the ionic or membrane phase potential. The standard potentials for the PEFC reactions are (Newman and Thomas-Alyea 2004)

$$\begin{aligned} U_h &= 0 \text{ for HOR} \\ &= 1.250 + 0.230\left(1 - \frac{T}{273.16}\right) \text{ for ORR} \end{aligned} \tag{28}$$

The parameters values related to Pt/C and NSTF reaction kinetics are available in the literature (Balliet and Newman 2011a, b, Ahluwalia et al. 2012).

Apart from the aforementioned transport processes, radiation heat transfer can take place. However, the operating temperatures of PEFCs are in the range of room temperature to about 80 °C. Thus the magnitude of the radiation heat transfer will be relatively smaller compared to the convective heat transfer from the cell surface to the surrounding. A simple correction of the overall convective heat transfer coefficient can take care of the convective-radiative heat transfer together.

5. Heat and Fluid Flow in Catalyst Layer and Gas-Diffusion Electrode

As the multi-component reactant gases are present throughout the CLs and the GDEs, the governing equations for each phase are needed to derive using a volume-averaging method. The basic principle of volume-averaging procedure for multi-phase flow is to average the single-phase conservation equation over an elementary volume, where several phases coexist.

5.1 Multi-phase volume-averaging method

When two or more miscible fluids occupy the void space of a porous layer, they mix because of diffusive and dispersive effects, leading ultimately to a multi-component mixture. In order to capture the interactions between the phases, a volume-averaging procedure can be applied to the conservation equations for each species. The volume-averaging procedure integrates the conservation equation for each species over a representative volume. For any quantity Ψ associated with phase *k* (can be liquid, gas or solid-phase) in PEFC porous media, the volume average of Ψ_k, which is also known as superficial average, can be defined as

$$\left\langle \Psi_k \right\rangle = \frac{1}{V_r} \int_{V_r} \Psi_k dV \tag{29}$$

where V_r is the representative volume and Ψ_k is taken to be zero in other phases. The representative volume is illustrated in Figure 16.8.

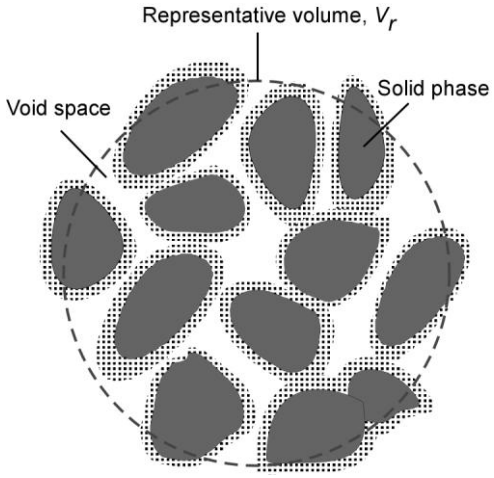

Figure 16.8 – Representative volume for volume-averaging method.

In addition to the superficial average term, the phase-volume or intrinsic average quantities can be defined as

$$\left\langle \Psi_k \right\rangle^k = \frac{1}{V_k} \int_{V_k} \Psi_k dV \tag{30}$$

where V_k is the representative volume of phase *k*. These two quantities (superficial average and intrinsic average) are related through

$$\frac{\left\langle \Psi_k \right\rangle}{\left\langle \Psi_k \right\rangle^k} = \frac{V_k}{V_r} = \varepsilon_k \tag{31}$$

in which ε_k is the volume fraction of phase *k* within the representative volume.

Using the volume average method, the governing volume-averaged equations for multi-phase transport processes for phase *k* (liquid, gas or solid-phase) can be written as follows (Whitaker 1971, Gray 1975, Kaviany 1995, Baschuk and Li 2005, Das 2010)

Conservation of mass:

$$\frac{\partial}{\partial t}\left(\varepsilon_k \left\langle \rho_k \right\rangle^k\right) + \nabla.\left(\varepsilon_k \left\langle \rho_k \right\rangle^k \left\langle \mathbf{v}_k \right\rangle^k\right) = \Gamma_{M,k} \tag{32}$$

Conservation of momentum:

$$\begin{aligned}\frac{\partial}{\partial t}\left(\varepsilon_k \left\langle \rho_k \right\rangle^k \left\langle \mathbf{v}_k \right\rangle^k\right) + \nabla.\left(\varepsilon_k \left\langle \rho_k \right\rangle^k \left\langle \mathbf{v}_k \right\rangle^k \left\langle \mathbf{v}_k \right\rangle^k\right) + \nabla\left(\varepsilon_k \left\langle p_k \right\rangle^k\right) \\ - \left\langle p_k \right\rangle^k \nabla\varepsilon_k - \nabla.\left(\varepsilon_k \left\langle \tau_k \right\rangle^k\right) - \varepsilon_k \left\langle \mathbf{b} \right\rangle^k = \Gamma_{F,k}\end{aligned} \tag{33}$$

Conservation of species:

$$\frac{\partial}{\partial t}\left(\varepsilon_k \left\langle \rho_k \right\rangle^k \left\langle \omega_k^\alpha \right\rangle^k\right) + \nabla.\left(\varepsilon_k \left\langle \rho_k \right\rangle^k \left\langle \omega_k^\alpha \right\rangle^k \left\langle \mathbf{v}_k \right\rangle^k + \varepsilon_k \left\langle \boldsymbol{J}_k^\alpha \right\rangle^k\right) = \Gamma_{S,k}^\alpha \tag{34}$$

Conservation of energy:

$$\begin{aligned}\frac{\partial}{\partial t}\left(\sum_k \sum_{\alpha \neq \alpha^\pm} \varepsilon_k \left\langle \rho_k \right\rangle^k \left\langle \omega_k \right\rangle^k C_{p,k}^\alpha \left\langle T \right\rangle^k\right) + \nabla.\left(\sum_k \sum_{\alpha \neq \alpha^\pm} \varepsilon_k \left\langle \boldsymbol{F}_\alpha^k \right\rangle^k C_{p,k}^\alpha \left\langle T \right\rangle^k\right) \\ = -\nabla.\left\langle q \right\rangle^k + Q_v + Q_{jle} + Q_{rxn}\end{aligned} \tag{35}$$

where the subscript *k* denotes the phase, τ_k is the viscous stress, **b** is the body force, ω_k^α is the mass fraction of species α within phase *k*, $\boldsymbol{J}_k^\alpha$ is the mass flux of species α due to molecular diffusion. The term $\left\langle T \right\rangle^k$ represents the equilibrium temperature of all co-existing phases and *Q* denotes the energy consumption or production (heating/cooling due to evaporation/condensation, Joule heating, and the heat of reaction). In the conservation of energy equation, the total mass flux of species α is defined as

$$\boldsymbol{F}_\alpha^k = \rho_k \omega_k^\alpha \mathbf{v}_k + \boldsymbol{J}_k^\alpha \tag{36}$$

In Eqs (32)-(34), the right-hand terms represent the source terms and each of these terms can vary based on each layer and phase. Moreover, these terms include the interfacial source terms (Baschuk and Li 2005).

5.2 Multi-phase mixture and two-fluid methods

There are two approaches widely used for the porous layers of PEFCs, namely, multi-phase mixture and two-fluid methods. In the first approach, it is considered that the gas and liquid phases are non-continuous and form a pseudo-fluid or multiphase mixture. Thus, all the transport equations can be divided into two groups. One will be applying for the multiphase mixture phase and the other for the solid phase. The main advantage of using a multi-phase

mixture approach is: it does not require to solve both liquid and gas phases and no approximation will be required for the interfacial source-terms, as they will be canceled out, except the solid-fluid interfacial source term. However, the multiphase mixture method requires a careful estimation of the properties of the mixture. Often the effective medium theory is used to estimate physicochemical properties of the multiphase mixture, which is, in fact, an approximation and can lead to erroneous results. The detailed explanation of the multiphase mixture, associated conservation equations, and mixture properties are available elsewhere (Baschuk and Li 2005).

In reality, both gas and liquid phases co-exist in the continuous phase inside the porous layers of a PEFC. Thus, the two-fluid (gas and liquid water) method can provide a more realistic picture of transports inside the porous layers of a PEFC. In the two-fluid method, both the gas and liquid phase conservation equations are required to solve together with appropriate approximations. One key approximation is required for the interfacial interaction between the gas and liquid phase. This can be simplified by considering the phase-change of liquid water (as liquid phase has only liquid-water) and assuming negligible interactions for the other species. In the following, a discussion is provided for the two-fluid method and related conservations equations for the GDEs and CLs.

5.2.1 Transport of gas phase

For the gas phase transport through the GDEs and CLs, we can recall Eqs (32)-(34) and replace phase *k* with gas phase (*g*). Thus, the conservations of mass, momentum, and species can be written as

$$\frac{\partial}{\partial t}\left(\varepsilon_g \rho_g\right) + \nabla.\left(\varepsilon_g \rho_g \mathbf{v}_g\right) = \Gamma_{M,g} \tag{37}$$

$$\frac{\partial}{\partial t}\left(\varepsilon_g \rho_g \mathbf{v}_g\right) + \nabla.\left(\varepsilon_g \rho_g \mathbf{v}_g \mathbf{v}_g\right) + \nabla\left(\varepsilon_g p_g\right) - \nabla.\left(\varepsilon_g \boldsymbol{\tau}_g\right) = \Gamma_{F,g} \tag{38}$$

$$\frac{\partial}{\partial t}\left(\varepsilon_g \rho_g \omega_g^{\alpha}\right) + \nabla.\left(\varepsilon_g \rho_g \omega_g^{\alpha} \mathbf{v}_g + \varepsilon_g \boldsymbol{J}_g^{\alpha}\right) = \Gamma_{S,g}^{\alpha} \tag{39}$$

For the momentum equation, the body force term is not applicable inside the PEFC porous media. For the species transport in the gas phase, an ideal three-component gas mixture

(water vapor, O_2, and N_2) should be considered for the cathode side and an ideal two-component gas mixture (water vapor and H_2) should be considered for the anode side.

Assuming the production of water in the cathode catalyst layer is in liquid form, the source terms for the conservation of mass equation in the GDEs (anode and cathode), cCL, and aCL are

$$\Gamma_{M,g} = \begin{cases} A\left(p_{\text{sat}} - x_g^{\text{H}_2\text{O}} p_g\right) & \in \text{ GDEs} \\ M_{\text{O}_2} A_v \dot{\wp}_{\text{O}_2} + A\left(p_{\text{sat}} - x_g^{\text{H}_2\text{O}} p_g\right) & \in \text{ cCL} \\ M_{\text{H}_2} A_v \dot{\wp}_{\text{H}_2} + A\left(p_{\text{sat}} - x_g^{\text{H}_2\text{O}} p_g\right) & \in \text{ aCL} \end{cases} \tag{40}$$

where p_{sat} is the saturation pressure, $x_g^{\text{H}_2\text{O}}$ is the water vapor mole fraction, M is the molecular weight, and $\dot{\wp}$ is the consumption of species in the catalyst layers (Baschuk and Li 2005). The term A represents a constant that represents the interfacial mass-transfer rate of water between the gas and liquid phases (Das 2010).

The source terms for the conservation of momentum equation can be simplified as a generalized Darcy term for GDEs and CLs as

$$\Gamma_{F,g} = -\frac{\varepsilon_g \mu_g}{K k_{rg}} \mathbf{v}_g \tag{41}$$

where μ_g is the viscosity of the gas mixture, K is the permeability, and k_{rg} is the relative permeability of the gas phase. Conversely, the source terms for the conservation of species equation are

$$\Gamma_{s,g}^{\text{H}_2\text{O}} = A\left(p_{sat} - x_g^{\text{H}_2\text{O}} p_g\right) \tag{42}$$

$$\Gamma_{s,g}^{\text{O}_2} = \begin{cases} 0 & \notin \text{ cCL} \\ M_{\text{O}_2} A_v \dot{\wp}_{\text{O}_2} & \in \text{ cCL} \end{cases} \tag{43}$$

$$\Gamma_{s,g}^{\text{H}_2} = \begin{cases} 0 & \notin \text{ aCL} \\ M_{\text{H}_2} A_v \dot{\wp}_{\text{H}_2} & \in \text{ aCL} \end{cases} \tag{44}$$

5.2.1 Transport of liquid phase

The liquid phase in PEFCs consists of liquid water only. Thus, the conservation of species is not required for the liquid water and the conservation of mass and momentum can be combined together for porous GDEs and CLs using Darcy's law, which gives

$$\frac{\partial}{\partial t}\left(\varepsilon_l \rho_l\right) + \nabla.\left(-\frac{\rho_l K k_{rl}}{\mu_l}\nabla p_l\right) = \Gamma_{M,l} \tag{45}$$

where k_{rl} is the relative permeability of liquid water. The liquid pressure inside the pores can be related to the gas pressure through the capillary pressure (p_c) as

$$p_c = p_l - p_g \tag{46}$$

The capillary pressure is also a function of liquid saturation (S_l), which is governed by the following expression (Das et al. 2011)

$$p_c = \gamma \cos\theta_c \left(\frac{\varepsilon}{K}\right) F\left(S_l\right) \tag{47}$$

where γ is the surface tension, θ_c is the contact angle, and $F(S_l)$ is the Leverett function (Leverett 1941). The Leverett function is mainly applicable to the packed beds and only includes the influence of porosity and permeability, but widely used for PEFCs. For GDEs and CLs, it is equally important to take account of wetting properties, such as breakthrough pressure and adhesion force (Das et al. 2012, Santamaria et al. 2014). Thus, the experimentally measured capillary pressure-saturation relationship should be considered for GDEs and CLs.

Using Eqs (46) and (47) in Eq (45), the liquid water transport equation can be expressed in terms of the liquid water saturation as,

$$\frac{\partial}{\partial t}\left(\varepsilon_l \rho_l\right) + \nabla.\left(-D_c \nabla S_l\right) = \Gamma_{S,l} \tag{48}$$

where D_c is the capillary diffusivity for the liquid water, which can be written as

$$D_c = \frac{K k_{rl}}{\mu_l}\rho_l \frac{dp_c}{dS_l} \tag{49}$$

The right-hand term of Eq (48) is

$$\Gamma_{S,l} = \begin{cases} -A\left(p_{\text{sat}} - x_g^{\text{H}_2\text{O}} p_g\right) + \nabla.\left(\rho_l \dfrac{k_{rl}}{\mu_l k_{rg}} \mathbf{v}_g\right) & \notin \text{ cCL} \\ M_{\text{O}_2} A_v \dot{\wp}_{\text{O}_2} - A\left(p_{\text{sat}} - x_g^{\text{H}_2\text{O}} p_g\right) + \nabla.\left(\rho_l \dfrac{k_{rl}}{\mu_l k_{rg}} \mathbf{v}_g\right) & \in \text{ cCL} \end{cases} \tag{50}$$

The last term in the above equation represents the amount of liquid water transport hindered by the gas flow, which can be neglected for the GDEs if the gas pressure is uniform.

5.2.1 Transport of energy

For the PEFCs porous media, it is realistic to assume that all phases will be in a local thermal equilibrium inside the pores, thus, the conservations of energy can be simplified as

$$\sum_{\alpha} \varepsilon_\alpha \rho_\alpha C_{p,\alpha} \left(\frac{\partial T}{\partial t} + \mathbf{v}_\alpha \cdot \nabla T\right) = \nabla.\left(k_T^{\text{eff}} \nabla T\right) + Q_v + Q_{\text{jle}} + Q_{\text{rxn}} \tag{51}$$

where k_T^{eff} is the effective thermal conductivity, which is a combination of the bulk thermal conductivities for the various phases. The source terms for Eq (51) can be expressed as

$$Q_v = \begin{cases} -\Delta H_v R_v & \in \text{GDEs} \\ -\Delta H_v \left(R_v + R_{v,M}\right) & \in \text{CLs} \end{cases} \tag{52}$$

$$Q_{jle} = \begin{cases} \dfrac{\mathbf{i}_s \cdot \mathbf{i}_s}{\sigma_s^{\text{eff}}} & \in \text{GDEs} \\ \dfrac{\mathbf{i}_s \cdot \mathbf{i}_s}{\sigma_s^{\text{eff}}} + \dfrac{\mathbf{i}_m \cdot \mathbf{i}_m}{\sigma_m^{\text{eff}}} & \in \text{CLs} \end{cases} \tag{53}$$

$$Q_{rxn} = \begin{cases} 0 & \in \text{GDEs} \\ i_h^{rxn}\left(\eta_h + \Pi_h\right) & \in \text{CLs} \end{cases} \tag{54}$$

where ΔH_v is the heat of vaporization, R_v is the rate of evaporation, $R_{v,M}$ is the rate of evaporation from the membrane, i_h^{rxn} is the overall rate reaction h, and Π_h is the Peltier coefficient (Weber and Newman 2006, Zenyuk, Das, and Weber 2016).

The governing conservation equations presented in this section only provide the transport of gas and liquid phases inside the GDEs and CLs. However, these transports processes are closely linked with the transports inside the membrane and the gas flow channels as well as the

transport of electron via the external circuit. Thus, the entire sets of transport equations are needed along with appropriate boundary conditions and related physicochemical properties to solve the governing conservation equations for the PEFCs. There are many studies available in the open literature that will provide the reader a clear idea of transports of mass, heat, electron, and protons in other layers of PEFCs and related boundary conditions (Weber et al. 2014).

6. Summary

This chapter summarizes, in brief, the transport processes involve in PEFC porous media (both GDEs and CLs). It provides insights to understand the structures of various components of PEFCs and the associated phases. The governing conservation equations provide an understanding of the transport conditions of gas and liquid phases inside the GDEs and CLs. The chapter highlights the vast complexities of transport within the polymer electrolyte fuel cells and the governing equations and transport properties for PEFCs are influenced by the physical structure of the cell and the co-existing phases.

Nomenclature

Abbreviation

aCL	- anode catalyst layer
aGDL	- anode gas diffusion layer
aMPL	- anode microporous layer
cCL	- cathode catalyst layer
cGDL	- cathode gas diffusion layer
cMPL	- cathode microporous layer
AEMFC	- anion-exchange-membrane fuel cells
GDE	- gas diffusion electrode
HOR	- hydrogen-oxidation reaction
ORR	- oxygen-reduction reaction
PEFC	- polymer-electrolyte fuel cell
PEMFC	- proton-exchange-membrane fuel cell

English

A_v - specific interfacial area, 1/m

A_s - catalyst surface area per unit mass of the catalyst, cm^2/mg

$c_{i,k}$ - concentration species *i* in phase *k*, $mole/m^3$

C_p - specific heat capacity, J/kg·K

D_i - Fickian diffusion coefficient of species *i*, m^2/s

$D_{i,j}$ - diffusion coefficient of *i* in *j*, m^2/s

F - Faraday's constant, 96487 C/equiv

i - current density, A/m^2

k_T - thermal conductivity, $J/m^2 \cdot K$

m_{Pt} - platinum loading, mg/cm^2

$\mathbf{N}_{i,k}$ - superficial flux density of species *i* in phase *k*, $mol/m^2 \cdot s$

p_i - partial pressure of species *i*, Pa

p_c - capillary pressure, Pa

p - pressure, Pa

q - heat flux, $J/m^2 \cdot s$

Q - source term for energy equation, $J/m^3 \cdot s$

R - ideal-gas constant, 8.31 J/mol·K

S_l - liquid saturation

Δs - entropy of reaction, J/mol·K

t - time, s

T - temperature, K

u_i - mobility of species *i*, $m^2 \cdot mol/J \cdot s$

U_h - reversible cell potential of reaction *h*, V

$\mathbf{v}$ - velocity vector, m/s

Greek

α_a - anodic transfer coefficient

α_c - cathodic transfer coefficient

δ - thickness, m

ε_k - volume fraction of phase *k*

ε - porosity

ρ_k - density of phase *k*, kg/m^3

σ - conductivity, S/m

η - overpotential, V

μ - viscosity, Pa·s

$\boldsymbol{\tau}$ - stress tensor, Pa

τ - tortuosity

ω_k - mass fraction of phase *k*

Φ - potential, V

Subscripts/Superscripts

CL - catalyst layer

eff - effective properties

g - gas phase

GDL - gas diffusion layer

i - arbitrary species

j - arbitrary species

k - arbitrary phase

l - liquid phase

m - membrane phase

ref - reference value

s - solid phase

Acknowledgments

The authors would like to thank Dr. Yasser Mahmoudi Larimi, Dr. Kamel Hooman, and Prof. Kambiz Vafai for the invitation to write this chapter. The financial support from the Engineering and Physical Sciences Research Council (EPSRC) via a research grant (EP/P03098X/1) is gratefully acknowledged. The authors also acknowledge the in-kind support of SGL CARBON GmbH and providing the GDL materials.

References

Ahluwalia, R. K., X. Wang, A. Lajunen, A. J. Steinbach, S. M. Hendricks, M. J. Kurkowski, and M. K. Debe. 2012. "Kinetics of oxygen reduction reaction on nanostructured thin-film platinum alloy catalyst." *Journal of Power Sources* 215:77-88.

Balliet, R. J., and J. Newman. 2011a. "Cold-start modeling of a polymer-electrolyte fuel cell containing an ultrathin cathode." *Journal of the Electrochemical Society* 158 (9):B1142-B1149.

Balliet, R. J., and J. Newman. 2011b. "Cold start of a polymer-electrolyte fuel cell i. Development of a two-dimensional model." *Journal of the Electrochemical Society* 158 (8):B927-B938.

Baschuk, J. J., and X. Li. 2005. "A general formulation for a mathematical pem fuel cell model." *Journal of Power Sources* 142 (1-2):134-153. doi: 10.1016/j.jpowsour.2004.09.027.

Das, P. K. 2010. "Transport phenomena in cathode catalyst layer of PEM fuel cells." Ph.D. thesis, University of Waterloo.

Das, P. K., A. Grippin, A. Kwong, and A. Z. Weber. 2012. "Liquid-water-droplet adhesion-force measurements on fresh and aged fuel-cell gas-diffusion layers." *Journal of the Electrochemical Society* 159 (5):B489-B496. doi: 10.1149/2.052205jes.

Das, P. K., X. Li, and Z. S. Liu. 2007. "Analytical approach to polymer electrolyte membrane fuel cell performance and optimization." *Journal of Electroanalytical Chemistry* 604 (2):72-90. doi: 10.1016/j.jelechem.2007.02.028.

Das, P. K., X. Li, and Z. S. Liu. 2008. "A three-dimensional agglomerate model for the cathode catalyst layer of PEM fuel cells." *Journal of Power Sources* 179:186-199. doi: 10.1016/j.jpowsour.2007.12.085.

Das, P. K., X. Li, and Z. S. Liu. 2010. "Effective transport coefficients in pem fuel cell catalyst and gas diffusion layers: Beyond Bruggeman approximation." *Applied Energy* 87 (9):2785-2796. doi: 10.1016/j.apenergy.2009.05.006.

Das, P. K., X. Li, Z. Xie, and Z. S. Liu. 2011. "Effects of catalyst layer structure and wettability on liquid water transport in polymer electrolyte membrane fuel cell." *International Journal of Energy Research* 35 (15):1325-1339. doi: 10.1002/er.1873.

Das, P. K., and A. Z. Weber. 2013. "Water management in PEMFC with ultra-thin catalyst-layers." *Proceedings of the ASME 11th Fuel Cell Science, Engineering, and Technology Conference* Paper No. FuelCell2013-18010:V001T01A002.

Debe, M. K. 2012. "Electrocatalyst approaches and challenges for automotive fuel cells." *Nature* 486 (7401):43-51. doi: 10.1038/nature11115.

Debe, M. K. 2013. "Tutorial on the fundamental characteristics and practical properties of nanostructured thin film (NSTF) catalysts." *Journal of the Electrochemical Society* 160 (6):F522-F534. doi: 10.1149/2.049306jes.

Gray, W. G. 1975. "A derivation of the equations for multiphase transport." *Chemical Engineering Science* 30 (2):229-233.

Holdcroft, S. 2014. "Fuel cell catalyst layers: A polymer science perspective." *Chemistry of Materials* 26 (1):381-393. doi: 10.1021/cm401445h.

Hwang, G. S., and A. Z. Weber. 2012. "Effective-diffusivity measurement of partially-saturated fuel-cell gas-diffusion layers." *Journal of the Electrochemical Society* 159 (11):F683-F692. doi: 10.1149/2.024211jes.

Kaviany, M. 1995. *Principles of heat transfer in porous media*. New York: Springer.

Leverett, M. C. 1941. "Capillary behavior in porous solids." *Petroleum Division Transactions of the American Institute of Mining and Metallurgical Engineers* 142:152-169.

Li, X. 2006. *Principles of fuel cells*. New York: Taylor & Francis.

Machado, B. S., N. Chakraborty, and P. K. Das. 2017. "Influences of flow direction, temperature and relative humidity on the performance of a representative anion exchange membrane fuel cell: A computational analysis." *International Journal of Hydrogen Energy* 42 (9):6310–6323. doi: 10.1016/j.ijhydene.2016.12.003.

Machado, B. S., N. Chakraborty, M. Mamlouk, and P. K. Das. 2018. "A three-dimensional agglomerate model of an anion exchange membrane fuel cell." *Journal of Electrochemical Energy Conversion and Storage* 15:011004-1--011004-12. doi: 10.1115/1.4037942.

Mench, M. M. 2008. *Fuel cell engines*. Hoboken, New Jersey: John Wiley & Sons.

Nam, J. H., K. J. Lee, G. S. Hwang, C. J. Kim, and M. Kaviany. 2009. "Microporous layer for water morphology control in PEMFC." *International Journal of Heat and Mass Transfer* 52 (11-12):2779-2791. doi: 10.1016/j.ijheatmasstransfer.2009.01.002.

Newman, J. , and K. E. Thomas-Alyea. 2004. *Electrochemical systems*. 3rd ed. New York: John Wiley & Sons.

Nonoyama, N., S. Okazaki, A. Z. Weber, Y. Ikogi, and T. Yoshida. 2011. "Analysis of oxygen-transport diffusion resistance in proton-exchange-membrane fuel cells." *Journal of The Electrochemical Society* 158 (4):B416-B423.

Pasaogullari, U., P. P. Mukherjee, C. Y. Wang, and K. S. Chen. 2007. "Anisotropic heat and water transport in a PEFC cathode gas diffusion layer." *Journal of the Electrochemical Society* 154 (8):B823-B834. doi: 10.1149/1.2745714.

Santamaria, A. D., P. K. Das, J. C. MacDonald, and A. Z. Weber. 2014. "Liquid-water interactions with gas-diffusion-layer surfaces." *Journal of the Electrochemical Society* 161 (12):F1184-F1193. doi: 10.1149/2.0321412jes.

Weber, A. Z., S. Balasubramanian, and P. K. Das. 2012. *Proton exchange membrane fuel cells*. Edited by K. Sundmacher. Vol. 41, *Advances in chemical engineering*: Academic Press.

Weber, A. Z., R. L. Borup, R. M. Darling, P. K. Das, T. J. Dursch, W. B. Gu, D. Harvey, A. Kusoglu, S. Litster, M. M. Mench, R. Mukundan, J. P. Owejan, J. G. Pharoah, M. Secanell, and I. V. Zenyuk. 2014. "A critical review of modeling transport phenomena in polymer-electrolyte fuel cells." *Journal of the Electrochemical Society* 161 (12):F1254-F1299. doi: 10.1149/2.0751412jes.

Weber, A. Z., and J. Newman. 2006. "Coupled thermal and water management in polymer electrolyte fuel cells." *Journal of the Electrochemical Society* 153 (12):A2205-A2214.

Whitaker, S. 1971. "The transport equations for multi-phase systems." *Chemical Engineering Science* 28 (1):139-147.

www.legislation.gov.uk. 2008. "Climate change act." accessed September 2018. http://www.legislation.gov.uk.

www.theccc.org.uk. 2012. "Committee on climate change technical report." accessed September 2018. https://www.theccc.org.uk.

Xing, L., W. D. Shi, P. K. Das, and K. Scott. 2017. "Inhomogeneous distribution of platinum and ionomer in the porous cathode to maximize the performance of a PEM fuel cell." *Aiche Journal* 63 (11):4895-4910. doi: 10.1002/aic.15826.

Xing, L., Y. Wang, P. K. Das, K. Scott, and W. D. Shi. 2018. "Homogenization of current density of PEM fuel cells by in-plane graded distributions of platinum loading and GDL porosity." *Chemical Engineering Science* 192:699-713. doi: 10.1016/j.ces.2018.08.029.

Zamel, N., X. Li, J. Shen, J. Becker, and A. Wiegmann. 2010. "Estimating effective thermal conductivity in carbon paper diffusion media." *Chemical Engineering Science* 65 (13):3994-4006. doi: 10.1016/j.ces.2010.03.047.

Zenyuk, I. V., P. K. Das, and A. Z. Weber. 2016. "Understanding impacts of catalyst-layer thickness on fuel-cell performance via mathematical modeling." *Journal of the Electrochemical Society* 163 (7):F691-F703. doi: 10.1149/2.1161607jes.